Organic Electronics 106 (2022) 106507

Contents lists available at ScienceDirect

Organic Electronics

journal homepage: www.elsevier.com/locate/orgel

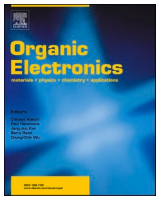

Using light-emitting complex Ir(mppy)$_3$ to detect acetone from 0.5 to 100 ppm by vertical-channel gas sensor

Chia-Hua Liu [a,1], Nguyen Pham Yen Nhi [a,1], Yi-Ming Sun [a], Hsin-Fei Meng [a,c,*], Hsiao-Wen Zan [b,**], Li-Yin Chen [b,***], Zheng-Hao Huang [b], Ya-Chung Tian [d,e], Chao-Sung Lai [e,f,g]

[a] Institute of Physics, National Yang Ming Chiao Tung University, Hsinchu, 300, Taiwan
[b] Department of Photonics and Institute of Electro-Optical Engineering, College of Electrical and Computer Engineering, National Yang Ming Chiao Tung University, 300, Taiwan
[c] Center for Emergent Functional Matter Science, National Yang Ming Chiao Tung University, Hsinchu, 300, Taiwan
[d] Department of Medicine, Chang Gung University, Taoyuan, 333, Taiwan
[e] Kidney Research Center and Department of Nephrology, Linkou Chang Gung Memorial Hospital, Taoyuan, 333, Taiwan
[f] Department of Electronic Engineering, Bio-drift Medical Research Center and Green Technology Research Center, Chang Gung University, Taoyuan, 333, Taiwan
[g] Department of Materials Engineering, Ming Chi University of Technology, New Taipei City, 243, Taiwan

ARTICLE INFO

Keywords:
Acetone
Iridium complex
Gas sensor
Breath

ABSTRACT

Acetone and ammonia are the gases in human breath with relatively high concentrations of 1–200 ppm and 0.5–2 ppm respectively. Gas sensors with vertical current channels covered with organic polymer semiconductors have been proved to have high sensitivity and reliability in breath ammonia detection. But the polymers have a large current drift in air and poor sensitivity to acetone. Here, the polymer is replaced by the iridium metal complex tris[2-(*p*-tolyl)pyridine]iridium(III), (Ir(mppy)$_3$), a common emitter in organic light-emitting diode (OLED). The vertical gas sensor now has good sensitivity to acetone in the important range of 0.5–100 ppm. The current of Ir(mppy)$_3$ sensor has a smaller drift in air during the measurement. In 800 s, the current drift of Ir(mppy)$_3$ device is only 3.2% percent, whereas the drift of PTB7 polymer device is 35% and P3HT polymer device is 29%. The good resolution of 0.5 ppm acetone is related to the stability of the current of Ir(mppy)$_3$ device.

1. Introduction

Breath detection has attracted a great interest recently for medical applications. It has the advantages of non-invasion and rapid outcome. For example, nitric oxide detection has been used for asthma [1–3], ammonia detection for kidney diseases [4,5], acetone detection for diabetes, and the combination of volatile organic compounds (VOC) detection is used for lung cancer [6]. Among all the components in breath asides from moisture and carbon dioxide, ammonia and acetone have by far the highest concentrations. The range of ammonia is from 0.5 ppm to 2 ppm [7], whereas the range of acetone is from 1 ppm to 200 ppm [8–10]. High level of breath ammonia concentration is a sign of kidney problems [11]. On the other hand, high breath acetone concentration may result from diabetes [12], fasting [9], and ketogenic diet [13]. Even though the medical diagnosis using breath acetone is still under study, it is widely accepted that acetone concentration is a key parameter in breath detection. The convenient acetone detector covering the important breath range of 1–100 ppm is desired. For high acetone concentrations over 20 ppm, gas detector tube can be used. For lower concentrations, electrochemical detectors are popular [14]. Electrochemical sensors have a long history and are commercially available, but they are relatively expensive and their lowest detection limit may not be enough for breath diagnosis.

There are many reports on acetone sensors using metal-oxide semiconductors [15,16]. The reported detection limit is 0.8–50 ppm at 200 °C [17]; 0.4–20 ppm at 200 °C [18]; 0.1 ppm at 220 °C [15] and 0.1 ppm at 365 °C [16]. One of the problems of metal oxide sensors is that the detection often requires a high temperature of over 200 °C for

* Corresponding author. Institute of Physics, National Yang Ming Chiao Tung University, Hsinchu, 300, Taiwan.
** Corresponding author.
*** Corresponding author.
E-mail addresses: meng@nycu.edu.tw (H.-F. Meng), hsiaowen@nycu.edu.tw (H.-W. Zan), lychen@nycu.edu.tw (L.-Y. Chen).
[1] Author contributions: Chia-Hua Liu and Nguyen Pham Yen Nhi contributed equally.

https://doi.org/10.1016/j.orgel.2022.106507
Received 22 November 2021; Received in revised form 22 March 2022; Accepted 25 March 2022
Available online 26 March 2022

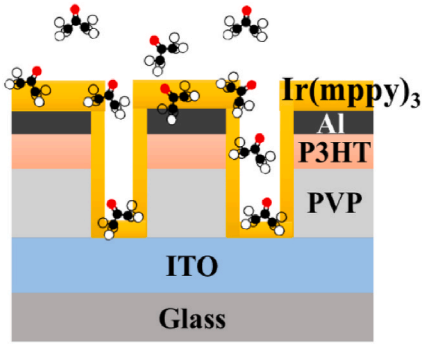

Fig. 1. Cross section of the vertical organic gas sensor. The diameter of the channel is 200 nm. The iridium complex Ir(mppy)$_3$ can detect the incoming acetone molecules by the current variation. 5 V is applied between ITO and Al electrodes. In the acetone molecule, oxygen is marked as red, carbon as black, and hydrogen as white.

reaction [15,16]. The heating system consumes power and raises the cost. In addition, the sol-gel fabrication of oxide semiconductors requires annealing at 200–400 °C. Such annealing temperature makes it difficult for fabrication on the convenient plastic substrate. Organic semiconductors have the advantages of room-temperature detection and low-temperature fabrication in solution. Gas sensors based on organic semiconductors have been reported to have a high sensitivity to ammonia, amines, and nitrogen oxides (NOx) [19]. Unfortunately, in general they seem to have a weak reaction to acetone. A possible reason is that acetone molecules have a low affinity to organic semiconductors. Clear response to 1 ppm of acetone is reported using the sandwich-type complexes [20,21]. The sensing material is complicated and the lower detection limit is still slightly too high.

In this work, we replace the conventional purely organic semiconductors by a common metal-organic complex in the organic gas sensor. Iridium complex has been well-known as the light-emitter for organic light-emitting diodes (OLED) [22]. The highest occupied molecular orbital (HOMO) and lowest unoccupied orbital (LUMO) involve the contributions from the heavy metal of iridium. It is quite different from the conventional organic semiconductor whose HOMO/LUMO levels contain contributions only from the pi-orbitals from carbon, nitrogen, or sulfur atoms. The overall charge density distributions are also quite different because the iridium atom is in an oxidized state. Due to these fundamental differences, the semiconducting iridium complex may have a higher affinity with acetone molecules which have a relatively higher dipole moment. Here the soluble iridium complex emitter is deposited as the sensing layer of the vertical-channel organic gas sensor [23]. Such vertical sensor has been shown to have a high sensitivity to ammonia down to 0.1 ppm [23–26]. When a green-emitting iridium complex Ir(mppy)$_3$ is used, the vertical sensor can detect acetone down to as low as 0.5 ppm. On the contrary, only 5 ppm can be detected when the conventional purely organic semiconductors are used in the same device structure. The detection range of 0.5–100 ppm of acetone is suitable for breath detection. Breath acetone detection by the convenient room-temperature organic semiconductor gas sensor is therein demonstrated using iridium complex in the vertical-channel structure.

2. Experimental methods

2.1. Material and sensor fabrication

The gas sensor was fabricated by the following processes and the structure is shown in Fig. 1. Similar steps have been reported previously for ammonia sensor [23–26].

Firstly, the indium-tin-oxide (ITO) glass substrates with the designed pattern are cleaned by acetone, isopropyl alcohol (IPA) and deionized water for 10 min. ITO is treated with oxygen plasma (100 W, 600 s) to form a hydrophilic surface. A cross-linkable poly (4-vinyl phenol) (PVP) insulation layer, with a thickness of about 300 nm, is spin-coated on the substrate at 3500 rpm and annealed at 200 °C for 1 h. A thin layer poly (3-hexylthiophene) (P3HT) (1.5 wt% in chlorobenzene) is then spin-coated on the PVP layer at 5000 rpm and annealed at 200 °C for 10 min. The P3HT modification layer absorbs the polystyrene (PS) nano-spheres (Fluka, 200 nm diameter) with good adhesion of negative charge. After the P3HT layer is coated, it is spin-rinsed with p-xylene at 5000 rpm. The substrate is immersed in PS solution (10 wt% in ethanol) for 90 s and dipped into boiling IPA for 10 s to remove excess PS spheres. Nitrogen flow is immediately applied to dry the substrate. Aluminum of 60 nm is deposited by a thermal evaporator. 3 M scotch tape is then used to remove the PS nano-spheres. An aluminum top electrode with a high density of the nano-spheres is prepared. PVP in the openings of the top electrode is dry-etched to form the cylindrical nano-pore vertical structure. Finally, blade coating is used with tris[2-(p-tolyl)pyridine] iridium(III) (Ir(mppy)3) (0.5 wt% in chlorobenzene) to form the sensing layer and annealed at 80 °C for 10 min. The blade speed is 25 mm/s unless otherwise specified. Two polymers are compared as the sensing materials, they are poly {4,8-bis [(2-ethylhexyl) oxy] benzo [1,2-b:4,5-b'] dithiophene-2,6-diyl- alt-3-fluoro-2-[(2-ethylhexyl) carbonyl] thieno [3,4-b] thiophene-4,6-diyl}(PTB7) and poly(3-hexylthiophene) (P3HT). The chemical structures of the materials are shown in Fig. 2. The HOMO

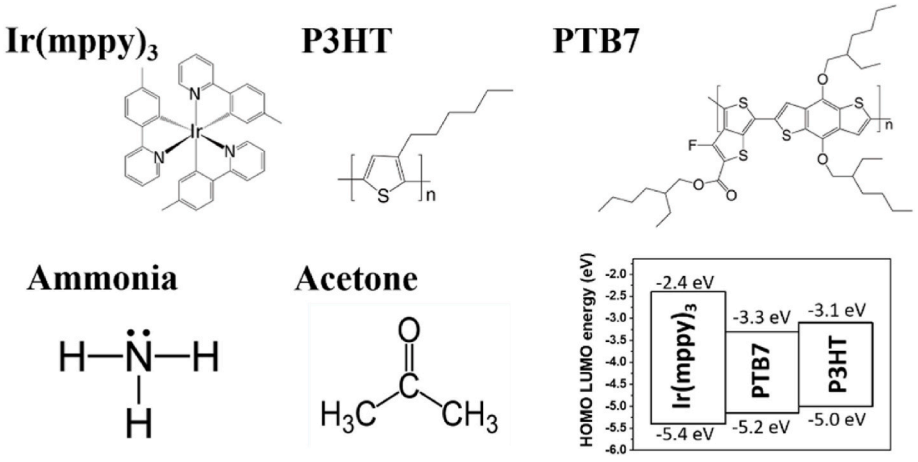

Fig. 2. Chemical structures of the Ir(mppy)$_3$, P3HT, PTB7, and the gas molecules ammonia and acetone. The HOMO/LUMO levels of the organic semiconductors are shown in eV relative to the vacuum level.

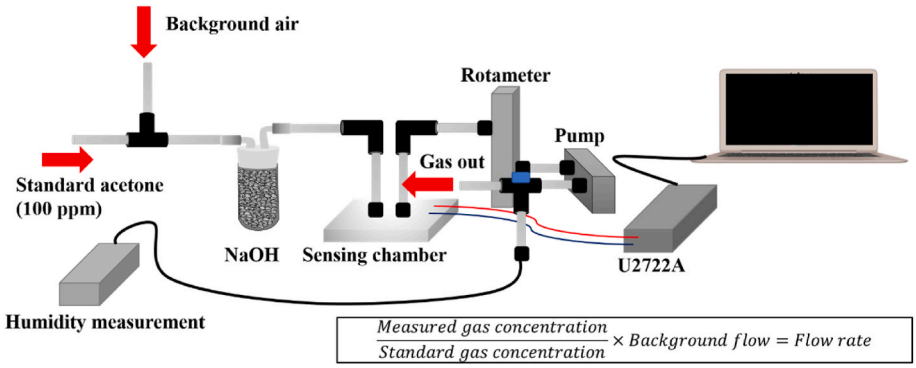

Fig. 3. Schematic view of the measurement system. The standard acetone has 100 ppm concentration from a gas cylinder. Measured concentration is obtained by mixing with air at certain flow rates. The current versus time is measured by the U2722A meter. NaOH dryer removes the air moisture.

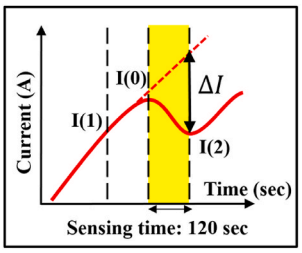

$$\Delta I = \big(I(2) - I(0)\big) - \big(I(0) - I(1)\big)$$

$$R = \frac{\Delta I}{I(0)} \times 100\%$$

Fig. 4. The schematic illustration of sensing response calculation. Extrapolation of the baseline is used to calculate the change ΔI. The response R is the percent of current change in 120 s of acetone exposure. The yellow area is the exposure time.

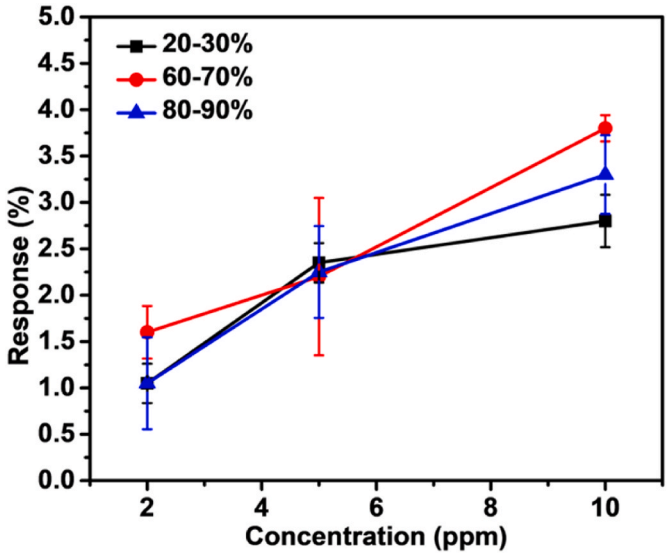

Fig. 5. Check for acetone responses with different relative humidities of background air. The low relative humidity level is 20–30%, the middle humidity level is 60–70%, the high humidity level is 80–90%.

and LUMO levels relative to the vacuum are shown in eV for the organic semiconductors as the sensing materials.

2.2. Measurement system

The measurement system is shown in Fig. 3. The system contains a desiccation glass cylinder with sodium hydroxide (NaOH) in order to provide a stable relative humidity (about 10%) to prevent the interference by moisture. There is a sensing chamber containing the device, a rotameter to control the flow at 250 cc/min, a pump to provide the stable air flow. An electric signal measurement instrument (Keysight U2722A) is used to apply 5 V on the sensor and read out the electric current signal to the computer. A humidity sensor is used to check relative humidity during measurement. Acetone with a given concentration is obtained by mixing 100 ppm acetone from the gas cylinder and the air. A syringe controlled by a step motor is used. The syringe is first filled with 100 ppm acetone. The gas inside the syringe is then injected with a motor-controlled flow rate and mixed with the background air with the certain ratio as shown in Fig. 3. The measured gas concentration is determined by the ratio between the background air flow and the injection flow. The measurement is under room temperature around 24 °C–28 °C.

The sensing time was set as 120 s. The reaction response is calculated as in Fig. 4, the sensing response was defined by the ratio of the current variation to the initial current. The variation is calculated by the difference to the extrapolated baseline.

The effect of the background moisture is checked for acetone detection. In this work, the acetone with 100 ppm in nitrogen is mixed with the background room air to control the acetone concentration. The room humidity level changes daily. The NaOH dryer is expected to fix the relative humidity of the mixed gas before entering the Teflon sensing chamber. So the sensor response will not depend on the background relative humidity. In Fig. 5, the sensor responses for three background humidity levels are shown. The low relative humidity level is 20–30%, the middle humidity level is 60–70%, whereas the high humidity level is 80–90%. The high humidity is created by spraying some water in a bag, and the wet air in the bag is used as the background air. For the low humidity level, some NaOH powder is placed in a bag and the dry air inside the bag is used as the air background. The room air is at the middle level. Two sensors are measured for each humidity level. There is no statistical difference between the three humidity levels as shown in Fig. 5. Even though the high or low level of humidity is not precisely controlled by spraying water or adding NaOH, the results ensure that the acetone detection in this work is not affected by the background humidity at least for the range of 20–90% relative humidity.

3. Results and discussion

3.1. Acetone response from 100 to 0.5 ppm

The real-time current measurements of $Ir(mppy)_3$ sensor are shown in Fig. 6. The positive voltage is applied to ITO electrode. The current is measured every second under 5 V, and it was conducted at room temperature (24–28 °C). The yellow regions in the figure represent the acetone exposure times, which are 120 s each. The concentration of acetone changes from 0.5 ppm to 100 ppm. In Fig. 6(a), the current first decreased meaning that the sensor detected the acetone and after 120 s

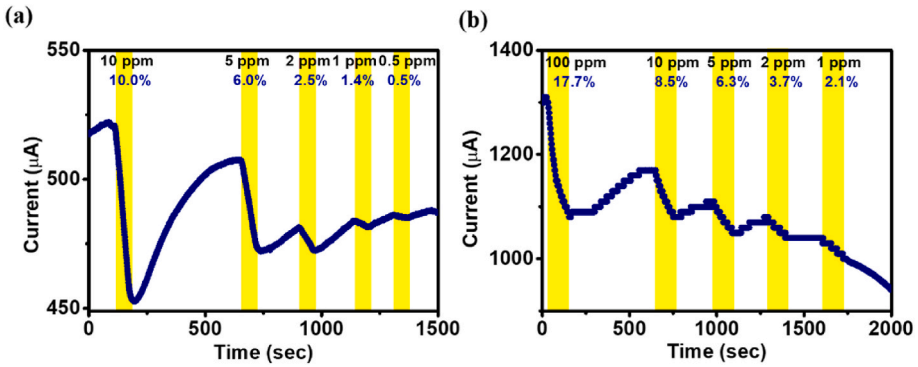

Fig. 6. (a) The real-time current response of $Ir(mppy)_3$ sensor under five exposures of acetone from 10 ppm down to 0.5 ppm. (b) The real-time current of $Ir(mppy)_3$ sensor under higher acetone concentration. The responses are indicated in percent. The yellow areas are the acetone exposure time of 120 s.

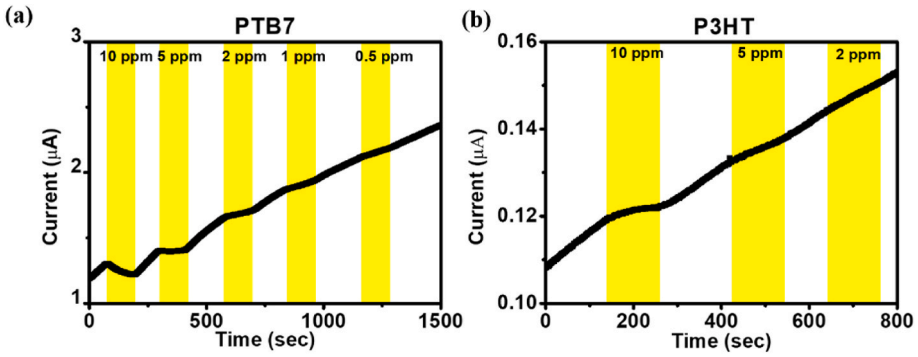

Fig. 7. (a) The real-time current sensing of PTB7 device under exposure to acetone. (b) The real-time current sensing of P3HT device under exposure of acetone. There is no exposure to 1 ppm and 0.5 p.m. for P3HT device because of the weak response.

the current started to recover. The responses of $Ir(mppy)_3$ sensor to the concentration of 10 ppm, 5 ppm, 2 ppm, 1 ppm and 0.5 ppm are 10%, 6.0%, 2.5%, 1.4% and 0.5%, respectively. Importantly, the slope of the current changes from positive to negative after $Ir(mppy)_3$ sensor is exposed to acetone as low as 0.5 ppm. Since the concentration of acetone in human breath can be to 200 ppm [9]. Acetone of 100 ppm is also measured and the response is 17.7% as shown in Fig. 6(b). The 100 ppm acetone is collected by the air bag directly from the gas cylinder without any dilution. The cylinder concentration is verified by the detector tubes. The result in Fig. 6 shows that the vertical sensor with $Ir(mppy)_3$ covers the entire wide range of breath acetone from 100 ppm down to 0.5 ppm. We did not go beyond 100 ppm because of the cylinder concentration limit.

The reaction between the sensing material and various gases is usually explained by the doping or de-doping effect of the gas molecules [23,27]. The organic semiconductors are usually p-type in air because of the ambient oxygen. When the organic semiconductor is exposed to air, the adsorbed oxygen molecules will cause electrons transfer from the valence band and leave mobile holes in the semiconductor. The negative charge on the oxygen atom of the C═O double bond in acetone gives a relatively strong dipole moment among common small molecules. The acetone dipole moment of 2.7 Debye (D) is much higher than 1.4 D for ammonia, 0.95 D for hydrogen sulfide, and 1.85 D for water. The negative charge of acetone may attract the mobile holes through Coulomb interaction. Once the holes are localized, the p-type conductivity of the semiconductor is reduced. Ammonia gas may have a similar sensing mechanism through the negative charge on the lone pair electrons.

There is another possible acetone sensing mechanism [28]. The adsorbed oxygen molecule may capture an electron and become negatively charged as O_2^-. Acetone is usually classified as a reducing gas. So the acetone molecule may associate with O_2^- and reduce it back to O_2. The electrons are released back to the organic semiconductors to neutralize the mobile holes. The p-type electrical current is therefore reduced. In general, the gas is attached to the organic semiconductor by mostly physical adsorption. When the exposure stops, the gas molecules will leave the semiconductor surface and the current will gradually return to the initial value.

The acetone response of the metal complex device is compared with the devices using polymers reported before. Two polymers are selected, they are PTB7 and P3HT. The sensor device fabrication is similar to Ir $(mppy)_3$. In the last step of sensing material coating, PTB7 was deposited by blade-coating (200 mm/s) and annealed at 200 °C for 10 min. On the other hand, P3HT was deposited by spin-coating at 3000 rpm and annealed at 200 °C for 10 min. As shown in Fig. 7, PTB7 and P3HT have much weaker responses to acetone compared with $Ir(mppy)_3$ shown in Fig. 6. For low concentrations, there is only a barely observable change in the slope as a function of time. But the sign of the slope remains positive with or without acetone exposure. For PTB7 a negative slope is seen only for acetone concentration above 5 ppm, whereas for P3HT negative slope appears for acetone above 10 ppm. The weaker reaction of the polymers to acetone may be related to the near charge neutrality on the main chain. There is no site that will match and attract the dipole moment of acetone molecules by the dipole-dipole interaction. On the other hand, the iridium ion in $Ir(mppy)_3$ may give a suitable positive charge density for acetone attachment.

Once the organic semiconductor device is exposed to the air, the electrical current level is often unstable, i.e., a current drift. There is a general trend of current increase in air due to the p-doping by oxygen molecules. As discussed above once the oxygen molecules are adsorbed on the organic semiconductors, there will be electrons transferred from the semiconductors to the oxygen molecules due to the high electron affinity of oxygen. When the air exposure time increases, there are more and more adsorbed oxygen molecules and higher hole concentration.

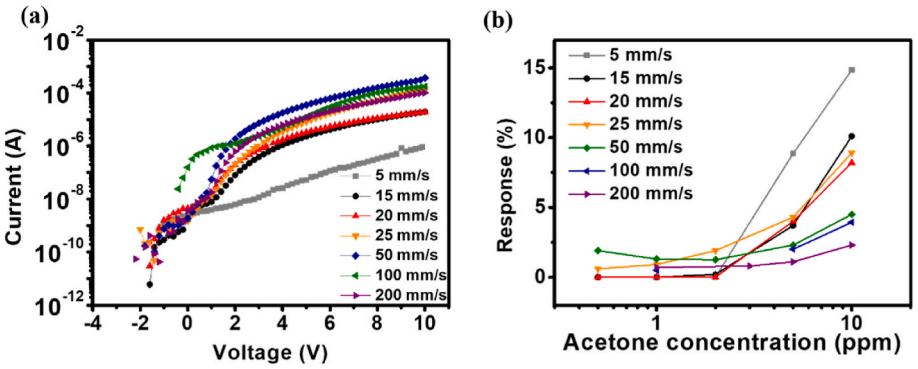

Fig. 8. (a) The current-voltage relation of $Ir(mppy)_3$ sensor made by different blade coating speeds of 200, 100, 50, 25, 20, 15, and 5 mm/s. (b) The acetone calibration curves for different blade-coating speeds. The acetone concentration is from 0.5 ppm to 10 ppm on the log scale.

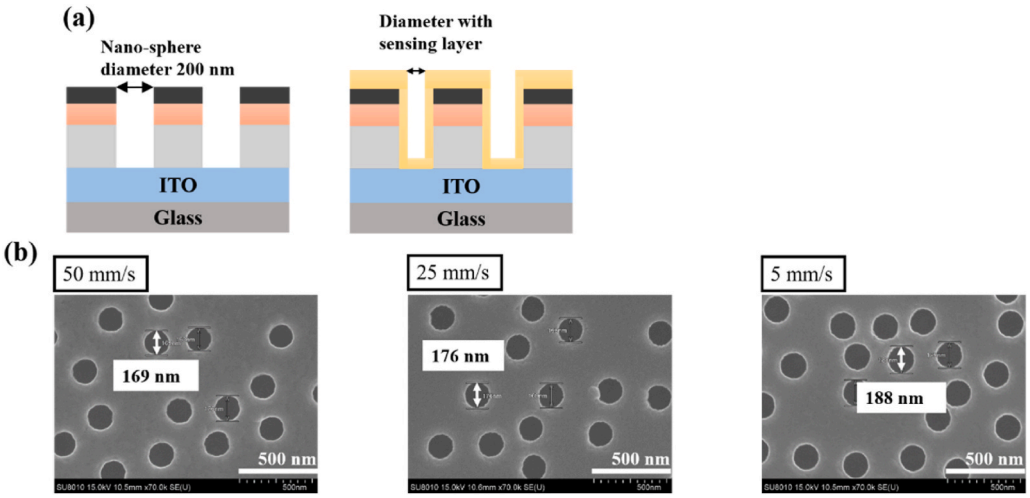

Fig. 9. (a) Cross section of the vertical channel covered with sensing layer marked in light orange. (b) The top-view SEM images of sensors with blade coating speeds 50, 25, 5 mm/s. The diameters in nm are given. The difference between the diameter and 200 nm is an estimate of the twice of sensing layer thickness.

The positive current drift for PTB7 and P3HT is significant as shown in Fig. 7. On the other hand, the drift is much smaller for $Ir(mppy)_3$. This suggests that the oxygen p-doping is less efficient in $Ir(mppy)_3$.

3.2. Optimizing the sensor fabrication

Below some parameters for the acetone devices are investigated. The response might be improved by tuning the thickness of the sensing layer [29]. The $Ir(mppy)_3$ sensors with the thinner film are prepared by reducing the blade coating speed and the concentration of $Ir(mppy)_3$ in chlorobenzene. For lower speed, the film is thinner. But the actual thickness on the side wall of the vertical channel cannot be measured. We therefore use the blade speed as the parameter for the thickness. The effect of the speed is shown in Fig. 8. The IV curves are shown in Fig. 8(a) for the speeds of 200 mm/s, 100 mm/s, 50 mm/s, 25 mm/s, 20 mm/s, 15 mm/s and 5 mm/s. Fig. 8(b) shows the acetone responses for various speeds. Thinner films are more sensitive. However, the level of electric current is another factor to be considered. In Fig. 8(b) the current greatly

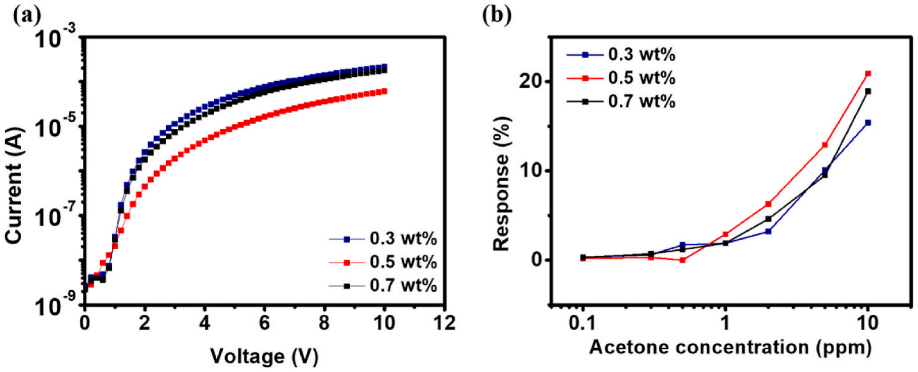

Fig. 10. (a) The current-voltage relation of $Ir(mppy)_3$ sensor made by different concentrations including 0.3 wt%, 0.5 wt% and 0.7 wt% in chlorobenzene solution. (b) The calibration curves of different concentrations.

Table 1
The relative current variations during 800 s in air for sensors of $Ir(mppy)_3$, PTB7 and P3HT. The latter two have much higher variations than the former.

	$Ir(mppy)_3$	PTB7	P3HT
Current variation (800 s)	$-9 \pm 2.7\%$	$47 \pm 1.7\%$	$30 \pm 7.3\%$

decreases to below 0.1 μA at 5 V when the blade coating speed comes down to 5 mm/s. When the current is too low, there will be lifetime and stability issues. Therefore, considering both the sensitivity and the current level, 25 mm/s is chosen as the optimal blade coating speed.

The effect of the blade coating speed on the sensing film coverage is illustrated in Fig. 9. After solution coating and drying the sensing film will cover both the top and the vertical side walls of the vertical channels as shown in Fig. 9 (a). The hole current flows from the bottom ITO to the Al, labeled as black, upward inside the vertical channel. It is difficult to measure film thickness inside the channel. So we use the scanning electron microscope (SEM) from the top to estimate. Without the sensing film, the channel diameter is 200 nm as shown on the left of Fig. 9(a). After the film coating, the diameter is reduced by roughly twice the film thickness as shown in the right of Fig. 9(a). In Fig. 9 (b) the SEM images for three coating speeds are shown. Indeed, for higher speed, the diameter is smaller because the film is thicker on the side wall. In particular, the film thickness is estimated as (200-169)/2 = 15.5 in nanometer for the speed of 50 mm/s.

Next, the effect of the concentration of $Ir(mppy)_3$ in chlorobenzene solution is studied. The results for 10, 5, 2, 1 and 0.5 ppm acetone, the calibration curve, and I–V curve without acetone are shown in Fig. 10. It shows that the calibration curves of 0.5% wt% are higher than 0.3% and 0.7%. Consequently, the optimal fabrication condition of $Ir(mppy)_3$ is 25 mm/s for blade coating speed with 0.5 wt% chlorobenzene solution. The sensing film thickness generally increases with the solution concentration. When the concentration is too small, there are not enough sensing materials on the vertical side walls. On the other hand, when the concentration is too high the film is too thick so only a small part of that is affected by the acetone molecules. There is therefore an optimal concentration.

3.3. Comparing 10-min stability for $Ir(mppy)_3$, PTB7 and P3HT

For $Ir(mppy)_3$, the current level remains roughly constant during the period of a few measurements, which is about 10 min in total. On the contrary, the current level keeps rising for the polymer devices with PTB7 and P3HT as shown in Fig. 7. The stable current level is strongly related to the ability to change the sign of slope upon acetone exposure when the current is plotted against time.

In Table 1, the percent of current variation in 800 s (roughly 13 min) are compared for the iridium complex $Ir(mppy)_3$ and polymers PTB7 and P3HT. The mean and standard deviations are obtained from three devices of the same material. The polymers both have a high percentage of $47 \pm 1.7\%$ and $30 \pm 7.3\%$ respectively, due to their higher background current rise than $Ir(mppy)_3$. Such a rise prevents the resolution of acetone signals at low concentrations. When the current increase rapidly, the exposure to acetone cannot reverse the trend of the current. On the other hand, the iridium complex $Ir(mppy)_3$ has a low percentage of $-9 \pm 2.7\%$ in 800 s in air. With a flat background current, the slope will change sign easily under the exposure to acetone for good resolution at low concentrations below 2 ppm. The 10-min air stability is unrelated to the HOMO levels given in Fig. 2. Somehow the ambient oxygen creates background p-doping more rapidly in the polymers than in the iridium complexes. The rate of oxygen p-doping turns out to be important to acetone detection.

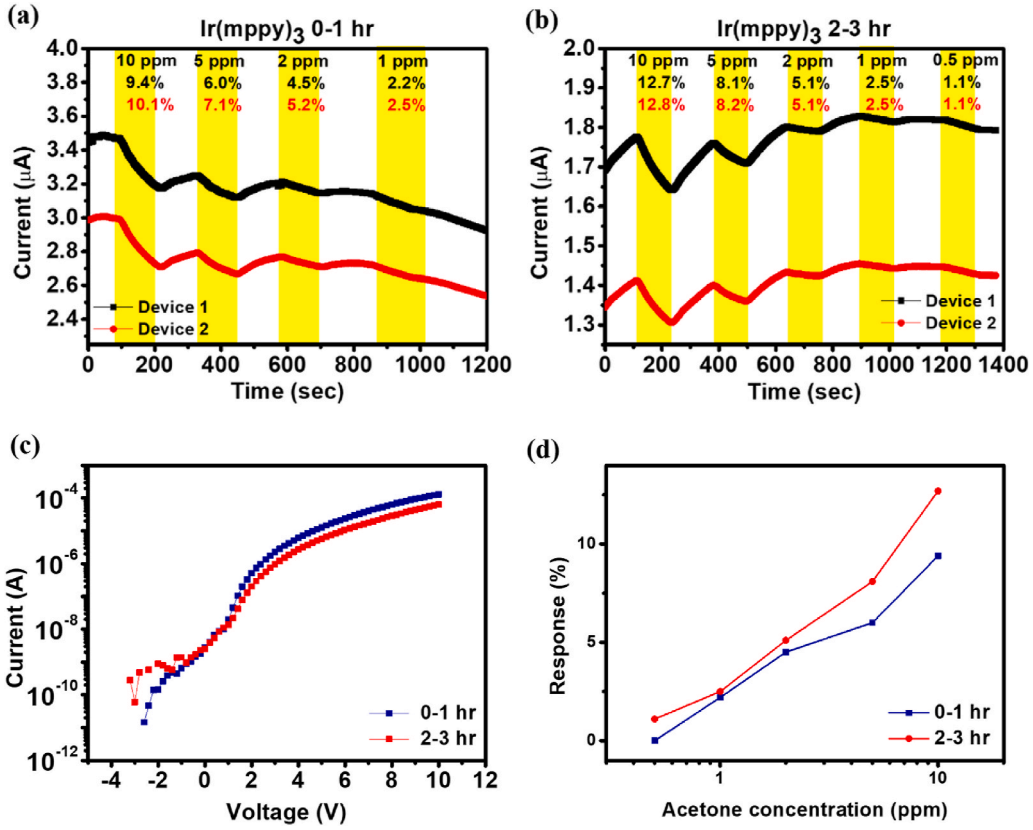

Fig. 11. (a)The real-time current sensing of $Ir(mppy)_3$ device under exposure of acetone for 0–1 h. (b)The real-time current sensing of $Ir(mppy)_3$ device under exposure of acetone for 2–3 h. In 1–2 h the device is stored in nitrogen. The behaviors for two samples are shown together. (c) The electric characteristic for 0–1 h and 2–3 h. (d) The calibration curves for 0–1 h and 2–3 h.

3.4. Tracing within 3 h

To evaluate a gas sensor, the time window with the reliable outcome is a critical parameter. So the sensor responses are compared before and after 1 h of storage. The sensor is tested with 10, 5, 2, 1 and 0.5 ppm acetone to establish the calibration curve and I–V relation before and after the storage. The sensing response measurement was done in ambient air. The result for the acetone real-time response is shown in Fig. 11(a), the calibration curve is shown as the 0–1 h curve in Fig. 11 (d), and the initial IV is shown as the 0–1 h curve in Fig. 11 (c). After that, we waited for 1 h. Within this hour the sensor was packaged by aluminum foil and stored in the vacuum tower at the room temperature. After the waiting hour the sensor is measured again in air. The real-time response is shown in Fig. 11(b), the calibration is shown as the 2–3 h curve in Fig. 11(d), and the IV curve is shown as the 2–3 h curve in Fig. 11(c). The entire time is about 3 h including two sets of air tests and the vacuum storage. The $Ir(mppy)_3$ sensor has a similar sensitivity to acetone over 3 h. Though the current drops, the calibration curves are similar. This suggests that the sensor can endure the ambient air during practical measurements for a few hours. This makes the $Ir(mppy)_3$ acetone sensor possible for practical applications.

The human breath acetone concentration covers a wide range from 1 ppm to 200 ppm. There are roughly three levels [9]. The low level is around 2 ppm, the middle level is between 2 ppm and 50 ppm, and the high level is over 50 ppm. For application as a rapid screening tool, the current acetone resolution is good enough to distinguish the levels despite of the variation. For more quantitative applications, more study is needed to reduce the variations of the device performances.

4. Conclusion

Using the common OLED emitter $Ir(mppy)_3$ as the sensing organic semiconductor, the vertical-channel gas sensor has a good resolution of acetone from 100 ppm down to 0.5 ppm. The gas sensor can be used to detect acetone in human breath, usually in the range of 1–200 ppm. Acetone levels in breath are related to health conditions including diabetes and obesity. The acetone sensor based on the iridium complex $Ir(mppy)_3$ is operated at room temperature. The current remains stable during measurement in air and the acetone concentration can be obtained in 2 min. It is therefore convenient to use in medical diagnosis.

Declaration of competing interest

The authors declare that they have no known competing financial interests or personal relationships that could have appeared to influence the work reported in this paper.

Acknowledgement

This work was supported by the Ministry of Science and Technology of the Republic of China under grant No. MOST 109-2811-M-009 -567.

References

[1] F.L.M. Ricciardolo, Revisiting the role of exhaled nitric oxide in asthma, Curr. Opin. Pulm. Med. 20 (2014) 53–59.
[2] T. Nagasaki, H. Matsumoto, Y. Kanemitsu, K. Izuhara, Y. Tohda, T. Horiguchi, H. Kita, K. Tomii, M. Fujimura, A. Yokoyama, Y. Nakano, S. Hozawa, I. Ito, T. Oguma, Y. Izuhara, T. Tajiri, T. Iwata, J. Ono, S. Ohta, T. Yokoyama, A. Niimi, M. Mishima, Using exhaled nitric oxide and serum periostin as a composite marker to identify severe/steroid-insensitive asthma, Am. J. Respir. Crit. Care Med. 190 (2014) 1449–1452.
[3] P.J. Honkoop, R.J.B. Loijmans, E.H. Termeer, J.B. Snoeck-Stroband, W.B. van den Hout, M.J. Bakker, W.J.J. Assendelft, G. ter Riet, P.J. Sterk, T.R.J. Schermer, J. K. Sont, Symptom-and fraction of exhaled nitric oxide–driven strategies for asthma control: a cluster-randomized trial in primary care, J. Allergy Clin. Immunol. 135 (2015) 682–688.
[4] S. Davies, P. Spanel, D. Smith, Quantitative analysis of ammonia on the breath of patients in end-stage renal failure, Kidney Int., 52(1) 1997 223- 228.
[5] A. Manolis, The diagnostic potential of breath analysis, Clin. Chem. 29 (1) (1983) 5–15.
[6] Z. Jia, A. Patra, V.K. Kutta, T. Venkatesan, Critical review of voltage organic compounds analysis in breath and in vitro call culture for detection of lung cancer, Metabolites 9 (2019) 52.
[7] T.L. Mathew, P. Pownraj, S. Abdulla, B. Pullithadathil, Technologies for clinical diagnosis using expired human breath analysis, Diagnostics 5 (2015) 27–60.
[8] S.J. Choi, I. Lee, B.H. Jang, D.Y. Young, W.H. Ryu, C.O. Park, I.D. Kim, Selective diagnosis of diabetes using Pt-functionalized WO3 hemitube networks as a sensing layer of acetone in exhaled breath, Anal. Chem. 85 (2013) 1792–1796.
[9] J.C. Anderson, Measuring breath acetone for monitoring fat loss: review, Obesity 23 (2015) 2327–2334.
[10] C. Deng, J. Zhang, X. Yu, W. Zhang, X. Zhang, Determination of acetone in human breath by gas chromatography-mass spectrometry and solid-phase microextraction with on-fiber derivatization, J Chromatogr B Analyt Technol Biomed Life Sci 810 (2014) 269–275.
[11] S. Davies, P. Spanel, D. Smith, Quantitative analysis of ammonia on the breath of patients in end-stage renal failure, Kidney Int. 52 (1) (1997) 223–228.
[12] M.P. Kalapos, Possible physiological roles of acetone metabolism in humans, Med. Hypotheses 53 (3) (1999) 236–242.
[13] O. Alkedeh, R. Priefer, The ketogenic diet: breath acetone sensing Technology, Biosensors 11 (2021) 26.
[14] N.K.R. Bogireddy, S.E.S. Rios, V. Agarwal, Simple one step synthesis of dual-emissive heteroatom doped carbon dots for acetone sensing in commercial products and Cr (VI) reduction, Chem. Eng. J. 414 (2021) 1.
[15] X. Wang, T. Wang, G. Si, Y. Li, S. Zhang, X. Deng, X. Xu, Oxygen vacancy defects engineering on Ce-doped α-Fe_2O_3 gas sensor for reducing gases, Sens. Actuators, B 302 (2020), 127165.
[16] P. Wang, T. Dong, C. Jia, P. Yang, Ultraselective acetone-gas sensor based ZnO flowers functionalized by Au nanoparticle loading on certain facet, Sensor. Actuator. B 288 (2019) 1–11.
[17] X. Zhou, J. Liu, C. Wang, P. Sun, X. Hu, X. Li, K. Shimanoe, N. Yamazoe, G. Lu, Highly sensitive acetone gas sensor based on porous ZnFe2O4 nanospheres, Sensor. Actuator. B 206 (2015) 577–583.
[18] K.W. Kao, M.C. Hsu, Y.H. Chang, S. Gwo, J.A. Yeh, A sub-ppm acetone gas sensor for diabetes detection using 10 nm thick ultrathin InN FETs, Sensors 12 (2012) 7157–7168.
[19] J. Brunet, M. Dubois, A. Pauly, L. Spinelle, A. Ndiaye, K. Guerin, C. Varenne, B. Lauron, An innovative gas sensor system designed from a sensitive organic semiconductor downstream a nanocarbonaceous chemical filter for the selective detection of NO2 in an environmental context Part I: development of a nanocarbon filter for the removal of ozone, J. Brunet et al. Sensor. Actuator. B 173 (2012) 659–667.
[20] P. Zhu, S. Li, X. Jiang, Q. Wang, F. Fan, M. Yan, Y. Zhang, P. Zhao, J. Yu, Noninvasive and wearable respiration sensor based on organic semiconductor film with strong electron affinity, Anal. Chem. 91 (2019) 10320–10327.
[21] X. Tang, Q. Liu, C. Wei, X. Lv, Z. Jin, Y. Chen, Advances in gas sensors of tetrapyrrolato-rare earth sandwich-type complexes-Commemorating the 100th anniversary of the birth of Academician Guangxian Xu, J. Rare Earth 39 (2021) 113–120.
[22] H.J. Bolink, E. Coronado, S.G. Santamaria, M. Sessolo, N. Evans, C. Klein, E. Baranoff, K. Kalyanasundaram, M. Graetzel, M.K. Nazeeruddin, Highly phosphorescent perfect green emitting iridium(III) complex for application in OLEDs, Chem. Commun. (2007) 3276–3278.
[23] S.Y. Yu, T.W. Tung, H.Y. Yang, G.Y. Chen, C.C. Shih, Y.C. Lee, C.C. Chen, H.W. Zan, H.F. Meng, C.J. Lu, A versatile method to enhance the operational current of air Stable organic gas sensor for monitoring of breath ammonia in hemodialysis patients, ACS Sens. 4 (2019) 1023–1031.
[24] M.Y. Chuang, J.N. Chen, H.W. Zan, C.J. Lu, H.F. Meng, Modulated gas sensor based on vertical organic diode with blended channel for ppb-regime detection, Sensor. Actuator. B 230 (2016) 223–230.
[25] M.Y. Chuang, H.W. Zan, P. Yu, Y.C. Lai, H.F. Meng, Gas permeable silver nanowire electrode for realizing vertical type sensitive gas sensor, Org. Electron. 15 (2014) 2769–2774.
[26] W.L. Chang, C.C. Chang, Y.T. Lee, A.D.T. Thi, C.C. Chen, H.F. Meng, H.W. Zan, C. J. Lu, M. He, Gas emission from human skin positions detected by vertical-channel organic semiconductor sensor, Sensor. Actuator. B 343 (2021), 129994.
[27] D. Kwak, Y. Lei, R. Maric, Ammonia gas sensors: a comprehensive review, Talanta 204 (2019) 713–730.
[28] A.A. Baharuddin, B.C. Ang, A.S.M.A. Haseeb, Y.C. Wong, Y.H. Wong, Advances in chemiresistive sensors for acetone gas detection, Mater. Sci. Semicond. Process. 103 (2019) 104616–104634.
[29] J. Zhang, X. Liu, G. Neri, N. Pinna, Nanostructured materials for room-temperature gas sensors, Adv. Mater. 28 (5) (2016) 795–831.